



# Investigating the usefulness of satellite-derived fluorescence data in inferring gross primary productivity within the carbon cycle data assimilation system

E. N. Koffi<sup>1,a</sup>, P. J. Rayner<sup>2</sup>, A. J. Norton<sup>2</sup>, C. Frankenberg<sup>3</sup>, and M. Scholze<sup>4</sup>

<sup>1</sup>Laboratoire des Sciences du Climat et de l'Environnement (LSCE), UMR8212, Ormes des merisiers, 91191 Gif-sur-Yvette, France

<sup>2</sup>School of Earth Sciences, University of Melbourne, Melbourne, Australia

<sup>3</sup>Jet Propulsion Laboratory, California Institute of Technology, Pasadena, USA

<sup>4</sup>Department of Physical Geography and Ecosystem Science, Lund University, Lund, Sweden

<sup>a</sup>now at: the European Commission Joint Research Centre, Institute for Environment and Sustainability, 21027 Ispra (Va), Italy

Correspondence to: E. N. Koffi (ernest.koffi@jrc.ec.europa.eu)

Received: 01 December 2014 – Published in Biogeosciences Discuss.: 13 January 2015

Revised: 18 June 2015 – Accepted: 18 June 2015 – Published: 07 July 2015

**Abstract.** Simulations of carbon fluxes with terrestrial biosphere models still exhibit significant uncertainties, in part due to the uncertainty in model parameter values. With the advent of satellite measurements of solar induced chlorophyll fluorescence (SIF), there exists a novel pathway for constraining simulated carbon fluxes and parameter values. We investigate the utility of SIF in constraining gross primary productivity (GPP). As a first test we assess whether SIF simulations are sensitive to important parameters in a biosphere model. SIF measurements at the wavelength of 755 nm are simulated by the Carbon-Cycle Data Assimilation System (CCDAS) which has been augmented by the fluorescence component of the Soil Canopy Observation, Photochemistry and Energy fluxes (SCOPE) model.

Idealized sensitivity tests of the SCOPE model stand-alone indicate strong sensitivity of GPP to the carboxylation capacity ( $V_{\text{cmax}}$ ) and of SIF to the chlorophyll AB content ( $C_{\text{ab}}$ ) and incoming short wave radiation. Low sensitivity is found for SIF to  $V_{\text{cmax}}$ , however the relationship is subtle, with increased sensitivity under high radiation conditions and lower  $V_{\text{cmax}}$  ranges.

CCDAS simulates well the patterns of satellite-measured SIF suggesting the combined model is capable of ingesting the data. CCDAS supports the idealized sensitivity tests of SCOPE, with SIF exhibiting sensitivity to  $C_{\text{ab}}$  and incom-

ing radiation, both of which are treated as perfectly known in previous CCDAS versions. These results demonstrate the need for careful consideration of  $C_{\text{ab}}$  and incoming radiation when interpreting SIF and the limitations of utilizing SIF to constrain  $V_{\text{cmax}}$  in the present set-up in the CCDAS system.

## 1 Introduction

The terrestrial carbon flux has been identified as the most uncertain term in the global carbon budget (Le Quéré et al., 2013). The gross primary productivity (GPP), which is the flux of  $\text{CO}_2$  assimilated by plants during photosynthesis, is the input to the system used to characterize carbon flux so its variation can significantly contribute to the uncertainties in terrestrial  $\text{CO}_2$  fluxes.

Complex systems have been built to reduce the uncertainties in GPP. These algorithms are either based on up-scaling or atmospheric inverse modelling methods. Up-scaling methods estimate GPP at global scale by establishing relationships between local GPP measurements and environmental variables then using these variables to calculate GPP globally (e.g., Jung et al., 2011; Beer et al., 2010 and references therein). The inverse modelling approach uses  $\text{CO}_2$  concentration observations at a global scale to constrain the pro-

cess parameters of carbon models that compute the terrestrial fluxes. This inverse method is an example of Carbon Cycle Data Assimilation Systems (CCDAS). The CCDAS considered in the present study has two main components:

- A deterministic dynamical model that computes the evolution of both the biosphere and soil carbon stores given an initial condition, forcing and a set of the model process parameters.
- An assimilation algorithm that allows the adjustment of a subset of the state variables, initial conditions and/or process parameters to reduce the mismatch between the model simulations and observations. Usually any prior information on the variables which are adjusted are also taken into account (see e.g., Kaminski et al., 2002, 2003; Rayner et al., 2005, and references therein for the underlying methodology).

Rayner et al. (2005) built such a CCDAS around the biosphere model BETHY (Biosphere Energy-Transfer Hydrology; Knorr, 2000) coupled to an atmospheric transport model together with CO<sub>2</sub> fluxes representing ocean flux, land use change, and fossil fuel emission, see also Scholze et al. (2007) and Kaminski et al. (2013) for an overview on further developments and applications. Koffi et al. (2012) used this CCDAS to investigate the sensitivity of estimates of GPP to transport models and observational networks of CO<sub>2</sub> concentrations. Large differences in GPP in the tropics were found between the GPP estimates of Koffi et al. (2012) and those from either satellite-based products or up-scaling methods (e.g., Jung et al., 2011; Beer et al., 2010). Koffi et al. (2012) found significantly larger GPP in the tropics compared to the other GPP products. In fact, due to few CO<sub>2</sub> concentration observations available in the tropics, the parameters of BETHY are mainly constrained by observations from other regions. Consequently, the optimized parameters can be uncertain.

Recent work has inferred sun-induced plant fluorescence (hereafter SIF) from the Greenhouse gas Observing Satellite (GOSAT; e.g., Frankenberg et al., 2011, 2012; Joiner et al., 2011; Guanter et al., 2012), ENVISAT/SCIAMACHY (Joiner et al., 2012), and MetOp-A/GOME-2 (Joiner et al., 2013). They showed that SIF data at a global scale is promising for inferring GPP. They found a strong linear correlation between satellite-based SIF and GPP estimated from either up-scaling methods (Jung et al., 2011) or satellite products (MODIS data). The satellite-based SIF data cover large areas of the globe including tropical zones where estimates from a CCDAS are found to be uncertain. It is worth asking whether such fluorescence data is useful to constrain GPP in the CCDAS framework.

The relationship between fluorescence and photochemistry at leaf level is reasonably well understood. Light energy absorbed by chlorophyll molecules has one of three fates: photosynthesis, dissipation as heat (non-photochemical

quenching) or chlorophyll fluorescence. The total amount of chlorophyll fluorescence is only 1 to 2 % of total light absorbed. The spectrum of fluorescence is different to that of absorbed light. The peak of the fluorescence spectrum lies between 650 and 850 nm. Under low-light conditions, a negative correlation has been found between fluorescence and photosynthesis light use efficiencies (e.g., Genty et al., 1989; Rosema et al., 1998; Seaton and Walker, 1990; Maxwell and Johnson, 2000; van der Tol et al., 2009a). At high-light conditions (i.e., high irradiance and moisture stress), a positive correlation has been observed between fluorescence and photosynthesis light use efficiencies (Gilmore and Yamamoto, 1992; Gilmore et al., 1994; Maxwell and Johnson, 2000; van der Tol et al., 2009a). Regarding the water stress, more recently, Lee et al. (2013) showed a negative correlation between vapour pressure deficit and SIF.

The cited works above show that the link between fluorescence and photosynthesis is complex. Thus, before using fluorescence observations to constrain gross primary productivity in the framework of CCDAS, first we need to ensure that there is a common parameter or set of parameters relevant to both the fluorescence and photosynthesis process models of the CCDAS. So, if there are common parameters, we can assess the sensitivities of GPP and SIF to them. This requires implementing in CCDAS a model that allows for the computing of both fluorescence and photosynthesis. We build such a CCDAS by using the SCOPE (Soil Canopy Observation, Photochemistry and Energy fluxes) model (van der Tol et al., 2009a, 2014). SCOPE is based on the existing theory of chlorophyll fluorescence and photosynthesis. The photosynthesis scheme of C<sub>3</sub> plants uses the formulations of Collatz et al. (1991), while for the C<sub>4</sub> photosynthesis pathway, the formulations of Collatz et al. (1992) are considered. In these formulations of the photosynthesis, the maximum carboxylation rate  $V_{\text{cmax}}$  is a key process parameter. The fluorescence model is based on the work of Genty et al. (1989), Rosema et al. (1998), and van der Tol et al. (2014). The model is formulated such that the sum of the probabilities of an absorbed photon to result in fluorescence, photochemistry, and heat is unity. Hence, the fluorescence model also utilizes  $V_{\text{cmax}}$  as a process parameter.

CCDAS operates in two modes (Scholze et al., 2007). The calibration mode that derives an optimal parameter set including posterior uncertainties of the dynamical carbon model (here the biosphere model) by constraining the process parameters of the model with observations. The diagnostic/prognostic (referred hereafter as forward) mode allows deriving the various quantities of interest (e.g., terrestrial carbon fluxes or atmospheric CO<sub>2</sub> concentrations) and their uncertainties. These quantities are calculated from the optimized parameter vector obtained from the calibration step. CCDAS has been widely applied to investigate terrestrial carbon cycling (e.g., Rayner et al., 2005; Scholze et al., 2007) and in particular more recently to (i) estimate the GPP at global scale (Koffi et al., 2012) and (ii) to quantify

the uncertainty in the parameters of BETHY by using both CO<sub>2</sub> concentration and flux observational networks (Kaminski et al., 2012; Koffi et al., 2013). To assess the usefulness of satellite-based fluorescence data (SIF) to constrain GPP within CCDAS, in this study, we investigate the sensitivities of both GPP and SIF to the biochemical parameters as well as environmental conditions by using the SCOPE model alone and the forward mode of the CCDAS built around it. The work is organized as follows: in Sect. 2, we describe both the model SCOPE and its coupling with CCDAS and the fluorescence data retrieved from the satellite GOSAT. In Sect. 3, we perform various idealized sensitivity tests to investigate the strength of the relationships between SIF and GPP by using the SCOPE model alone. These tests are performed by studying the sensitivity of GPP and SIF to the biochemical parameters (i.e.,  $V_{\text{cmax}}$  and the chlorophyll AB content  $C_{\text{ab}}$ ) and the environmental conditions (e.g., incoming short wave radiation  $R_{\text{in}}$ ). In the idealized tests, the vegetation is characterized by different values of the leaf area index (LAI). In Sect. 4, by using the forward mode of the CCDAS coupled to SCOPE, we compute both SIF and GPP at global scale and results are compared to the GOSAT SIF from June 2009 until December 2010. The simulations are based on the different settings of LAI,  $R_{\text{in}}$ ,  $V_{\text{cmax}}$ , and  $C_{\text{ab}}$  values. In Sect. 5, results are discussed. Finally, conclusions are presented in Sect. 6.

## 2 Models and data

### 2.1 Models

#### 2.1.1 SCOPE model

The model SCOPE is a 1-D model based on radiative transfer, micrometeorology, and plant physiology (van der Tol et al., 2009b). Version 1.53 of SCOPE is used in this study with the default version of the biochemical code (referred as fluorescence model choice 0; van der Tol et al., 2014). SCOPE treats canopy radiative transfer in the visible and infrared and chlorophyll fluorescence, as well as the energy balance. The modules of SCOPE are executed in the following order:

1. A semi-empirical radiative transfer model for incident sun and sky radiation, based on the SAIL model (Verhoef and Bach, 2007). This module calculates the outgoing radiation spectrum (0.4 to 50  $\mu\text{m}$ ) at the top of the canopy (hereafter TOC), as well as the net radiation and absorbed photosynthetically active radiation (aPAR) per surface element.
2. A numerical radiative transfer model for thermal radiation generated internally by soil and vegetation, based on Verhoef et al. (2007). This module computes the TOC outgoing thermal radiation and net radiation per surface element, but for heterogeneous leaf and soil temperatures.

3. A biochemistry model for C3 and C4 plants, which allows the computation of quantities relevant for photosynthesis and chlorophyll fluorescence at leaf level. At leaf level, the model calculates a fluorescence scaling factor relative to that of a leaf in low-light, unstressed conditions from absorbed radiative fluxes, canopy and ambient environmental conditions (radiation, temperature, air vapour pressure, CO<sub>2</sub>, and O<sub>2</sub> concentrations).
4. A radiative transfer model for chlorophyll fluorescence based on the FluorSAIL model (Miller et al., 2005) that calculates the TOC radiance spectrum of fluorescence over 640–850 nm from the geometry of the canopy and a calculated fluorescence spectrum that is linearly scaled by the leaf level chlorophyll fluorescence scaling factor.

In this study, SCOPE uses a canopy structure characterized by a spherical leaf angle distribution (parameters LIDF<sub>a</sub> and LIDF<sub>b</sub> in Table 1) as a function of LAI with 60 distributed elementary layers. The geometry of the vegetation is treated stochastically. SCOPE calculates the illumination of leaves with respect to their position and orientation in the canopy. The spectra of reflected and emitted radiation as observed above the canopy in the satellite observation direction are computed. It is worth noting that SCOPE permits variation only in the vertical dimension. Thus, it is valid for vegetation in which variations in the horizontal are smaller than in the vertical dimension. This is maybe a limitation for some natural canopies, especially when coupling to the CCDAS as performed in Sect. 2.1.2. However, the sensitivity of this limitation to the CCDAS results is beyond the scope of this study.

We briefly describe the fluorescence model at leaf level (more detail is given in van der Tol et al., 2009a, 2014) with focus on the variables and parameters relevant for the photosynthesis. The model of Faquahar et al. (1980) divides photosynthesis into two main processes: (1) regeneration of the ribulose biphosphate (RuP2), which depends on the light and (2) the maximum carboxylation rate at RuP2 saturated conditions in the presence of sufficient light. The regeneration of RuP2 for two photosystems (PSII and PSI) gives the link between photosynthesis and fluorescence.

As already mentioned above, the fluorescence model in SCOPE is formulated such that the sum of the probabilities of an absorbed photon to result in fluorescence, photochemistry, and heat is unity. Following this, the fluorescence  $\Phi_{\text{Ft}}$  from a single leaf is calculated over the spectrum window of 640–850 nm as follows:

$$\Phi_{\text{Ft}} = \Phi_{\text{Fm}} (1 - \Phi_{\text{p}}), \quad (1)$$

where  $\Phi_{\text{Fm}}$  is the fluorescence yield and computed as follows:

$$\Phi_{\text{Fm}} = \frac{K_{\text{f}}}{(K_{\text{f}} + K_{\text{d}} + K_{\text{n}})}. \quad (2)$$

With  $K_n$  being the rate coefficient relative to nonphotochemical quenching (NPQ), a parameter obtained from Pulse amplitude modulated (PAM) fluorometry. PAM measures the photosynthetic efficiency of photosystem II (PSII).  $K_n$  is parametrized by using Flexas et al. (2002)'s data set as follows:

$$K_n = (6.2473 \times x - 0.5944) \times x, \quad (3)$$

where  $x$  stands for the degree of light saturation and defined as:

$$x = 1 - \frac{\Phi_p}{\Phi_{p0}}. \quad (4)$$

$\Phi_p$  and  $\Phi_{p0}$  (given by the following expressions) stand for the fractions of actual and dark photochemistry yields, respectively:

$$\Phi_{p0} = \frac{K_p}{(K_f + K_d + K_p)}. \quad (5)$$

$K_f$  is the rate constant for fluorescence and sets to 0.05,  $K_p$  is the rate constant for photochemistry with a value of 4.0,  $K_d$ , with a value of 0.95, is the rate constant for thermal deactivation at  $\Phi_{Fm}$

$$\Phi_p = \Phi_{p0} \frac{J_a}{J_e}. \quad (6)$$

$J_a$  and  $J_e$  stand for the actual and potential electron transport rates, respectively.  $J_a$  is the electron transport rate used for gross primary productivity (GPP). van der Tol et al. (2014) used Pulse-Amplitude fluorescence measurements to derive an empirical relation between the efficiencies of photochemistry and fluorescence. This relationship was derived after analysing the response of non-photochemical quenching (NPQ) in plants to light saturation. The formulations of GPP in SCOPE follow that of Collatz et al. (1991) and Collatz et al. (1992) for C3 and C4 plants, respectively. The potential electron transport rate  $J_e$  is related to the rate of absorbed photons (or absorbed photosynthetically active radiation, i.e. aPAR), hence to the visible radiation. The fluorescence is linearly related to the short wave (visible) radiation, while it is related to  $V_{cmax}$  mainly when the gross primary productivity GPP is limited by the carboxylation enzyme Rubisco and the capacity for the export or the utilization of the products of photosynthesis.

The total top-of-canopy fluorescent radiance is obtained from the fluorescence flux (i.e.,  $\Phi_{Fi}$  in Eq. 1) and the spectral radiance of single leaves over all layers and orientations, taking into account the probabilities of viewing sunlit and shaded components. The model then calculates radiation transport in a multilayer canopy as a function of the solar zenith angle and leaf orientation to simulate fluorescence in the direction of satellite observation (van der Tol et al., 2009b).

Leaf biochemistry affects reflectance, transmittance, transpiration, photosynthesis, stomatal resistance, and chlorophyll fluorescence. Reflectance and transmittance coefficients, which are a function of  $C_{ab}$  are calculated by following the PROSPECT model (Jacquemoud and Baret, 1990). Two excitation fluorescence matrices (EF-matrices) representing fluorescence from both sides of the leaf are computed. The matrices convert a spectrum of aPAR into a spectrum of fluorescence. Details on the radiative transfer model of the fluorescence at the TOC level are given in van der Tol et al. (2009b).

### 2.1.2 Coupling SCOPE to CCDAS

Within CCDAS we replace the canopy radiative transfer and photosynthesis schemes of BETHY with their corresponding schemes from SCOPE and add the fluorescence model of SCOPE. The spatial resolution, vegetation characteristics as well as the meteorological and phenological data of BETHY are used to force SCOPE. The spatial resolution is  $2^\circ \times 2^\circ$  with 3462 land grid points for the globe. CCDAS uses 13 plant functional types (PFT; see Table 2), which have been derived by a condensation (grouping different crop types into one crop PFT) of the original 23 PFTs in BETHY (Knorr, 1997, based on Wilson and Henderson-Sellers, 1985). A grid cell can contain up to three different PFTs, with the amount specified by their fractional coverage.

## 2.2 Data

### 2.2.1 GOSAT fluorescence data

Frankenberg et al. (2011, 2012), Joiner et al. (2011), and Guanter et al., (2012) have published maps of SIF from GOSAT (Kuze et al, 2009). The retrieval measures terrestrial emission at the frequencies of solar Fraunhofer lines (gaps in the solar spectrum). Chlorophyll fluorescence is the main contributor to emissions at these frequencies. GOSAT carries a Fourier Transform Spectrometer (FTS) measuring with high spectral resolution in the 755–775 nm range, which allows resolving individual Fraunhofer lines overlapping the fluorescence emission. The method described in Frankenberg et al. (2011) makes use of two spectral windows centred at 755 and 770 nm to derive SIF. Results from the line centred around 755 nm for the period June 2009 to December 2010 are used in this study. The fluorescence data we are using are monthly means mapped onto  $2^\circ \times 2^\circ$  spatial resolution at global scale. The fluorescence product includes uncertainties.

### 2.2.2 Data relevant for models

The input data for the models we are using are of three main kinds: (i) the data for the canopy radiative transfer modules of SCOPE, (ii) the data characterizing the environmental conditions (i.e. meteorological and short and long wave radiation)

**Table 1.** SCOPE parameters.

Parameters	Symbol	Units	Range or values
Incoming short wave radiation	$R_{in}$	$W m^{-2}$	0–1200
Maximum carboxylation rate	$V_{cmax}$	$\mu mol m^{-2} s^{-1}$	1–250
Chlorophyll $a + b$ content	$C_{ab}$	$\mu g cm^{-2}$	1–80
Dry matter content	$C_{dm}$	$g cm$	0.012
Leaf equivalent water thickness	$C_w$	$cm$	0.009
Senescent material	$C_s$	/	0.0
Leaf structure	$N$	/	1.4
Leaf angle distribution parameter $a$	$LIDF_a$	/	–0.35
Leaf angle distribution parameter $b$	$LIDF_b$	/	–0.15
Leaf width	$w$	$m$	0.1
Ball-Berry stomatal conductance parameter	$m$	/	8
Dark respiration rate at 25 °C as fraction of $V_{cmax}$	$R_d$	/	0.015
Cowan's water use efficiency parameter	$k_c$	/	700
Leaf thermal reflectance	$\rho(\text{thermal})$	/	0.01
Leaf thermal transmittance	$\tau(\text{thermal})$	/	0.01
Soil thermal reflectance	$\rho_s(\text{thermal})$	/	0.06
Leaf area index LAI		/	0.1–6
fluorescence quantum yield efficiency at photosystem level	$f_{qe}$	/	0.02
Canopy height	$h_c$	$m$	1

**Table 2.** Main controlling parameters for the photosynthesis and fluorescence models are given.  $V_{cmax}$  stands for carboxylation maximum capacity and  $C_{ab}$  for the chlorophyll AB content for 13 plant functional types (PFT) as used in the CCDAS.

PFT number	Plant Function Type (PFT)	$V_{cmax}$ ( $\mu mol(CO_2) m^{-2} s^{-1}$ )		$C_{ab}$ ( $\mu g cm^{-2}$ )
		Prior value	Optimized values Koffi et al. (2012)	
1	Tropical broadleaved evergreen tree	60	63.8	40
2	Tropical broadleaved deciduous tree	90	73.5	15
3	Temperate broadleaved evergreen tree	41	39.7	15
4	Temperate broadleaved deciduous tree	35	149.2	10
5	Evergreen coniferous tree	29	21.9	10
6	Deciduous coniferous tree	53	136.4	10
7	Evergreen shrub	52	168.9	10
8	Deciduous shrub	160	96.1	10
9	C3 grass	42	18.9	10
10	C4 grass	8	0.7	5
11	Tundra	20	8.5	10
12	Swamp	20	9.3	10
13	Crop	117	47.9	20

relevant for both the canopy radiative transfer and biochemistry models, and (iii) the process parameters of the biochemistry models.

The model SCOPE requires incident radiation at the top-of-canopy as input. To take into account the atmospheric absorption bands properly, these data are needed at high resolution. The spectra of sun and sky fluxes at the top of the canopy are obtained from the atmospheric radiative transfer model MODTRAN (Berk et al., 2000). MODTRAN was run for 16 atmospheric situations representative of different re-

gions (Verhoef et al., 2014). We use 4 types of these generated atmospheres. They are tropical atmosphere for the tropical zones, winter and summer atmospheres for high and middle latitudes. In addition, we have at our disposal data for an atmosphere which is representative of the whole globe (hereafter standard atmosphere). We have tested the sensitivity of SIF and GPP to these four types of atmospheres. Results show only negligible differences between the inferred SIF and GPP. We consider the standard atmosphere for the ide-

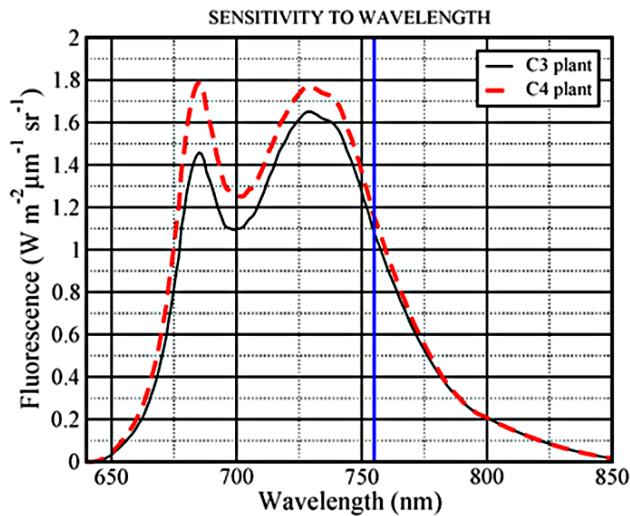


**Figure 1.** The simulated fluorescence (SIF) at the top of the canopy as a function of the radiation wavelength and for C3 (black solid line) and C4 (red dashed line) plants from the model SCOPE are shown, respectively. The blue solid line corresponds to wavelength value (i.e., 755 nm) at which the simulated SIF is calculated in this study, i.e., the equivalent of the satellite GOSAT based SIF.

alized tests (Sect. 4.1) and the seasonal atmosphere for the simulations at global scale by using the CCDAS (Sect. 4.2).

The system needs forcing data to drive SCOPE within the CCDAS framework. Monthly observed climate, incident radiation, and fractional soil moisture for the period 2009–2010 are used (Weedon et al., 2011). The LAIs are obtained from BETHY simulation.

The main parameters that affect both the photosynthesis and fluorescence schemes are given in Table 2. The parameters are of two kinds: parameters that are PFT-specific (e.g.,  $V_{\text{cmax}}$  and  $C_{\text{ab}}$ ) and global parameters. Prior and optimized values of  $V_{\text{cmax}}$  obtained by Koffi et al. (2012) are shown. The chlorophyll content  $C_{\text{ab}}$  is related to the nitrogen content of the leaf which itself is linked to the maximum rate of carboxylation through the proteins of the Calvin Cycle and the thylakoids. Some investigators have related the photosynthetic capacity of leaves of some specific plants to their nitrogen content (e.g., Evans, 1989; Kattge et al., 2009; Houborg et al., 2013). Other investigators have derived some empirical relationships between the nitrogen content and the chlorophyll content (e.g., Shaahan et al., 1999; van den Berg and Perkins, 2004; Ghasemi et al., 2011). Since the current version of the model SCOPE does not include the nitrogen scheme of a leaf, we first use the same value of chlorophyll content  $C_{\text{ab}}$  for all 13 PFTs. As a second step,  $C_{\text{ab}}$  values for each of the 13 PFTs are optimized so that the simulated SIF reproduces the main spatial characteristics of observed SIF.

### 3 Experimental set ups

#### 3.1 Idealized tests

We carry out some idealized sensitivity tests by using the SCOPE model alone. We investigate the sensitivity of SIF and GPP to biochemical parameters  $V_{\text{cmax}}$  and  $C_{\text{ab}}$ , environmental variables (atmospheric temperature and vapour pressure, etc), visible radiation, and LAI. We assume throughout the following sections the concentrations of both  $\text{CO}_2$  and  $\text{O}_2$  at the interface of the canopy to be constant. We will focus our discussions on the assessment of the sensitivity of the simulated SIF and GPP to  $V_{\text{cmax}}$ ,  $C_{\text{ab}}$ , LAI, and the short wave radiation. All the simulations in these tests are performed at noon.

We present a spectrum of simulated fluorescence for C3 and C4 plants in Fig. 1. Two peaks in the simulated fluorescence spectrum are shown at 680 and 725 nm. In agreement with van der Tol et al. (2009a), C4 plants exhibit larger SIF than C3 plants over the wavelength range 625 to 755 nm. These differences are amplified around the two peaks. We are using as observations the GOSAT satellite-derived SIF, which retrieved SIF around 755 nm. Therefore, the simulated fluorescence in this study corresponds to the SIF value at this wavelength. In Fig. 1, this is around  $1.2 \text{ W m}^{-2} \mu\text{m}^{-1} \text{ sr}^{-1}$ .

For all of the idealized tests presented hereafter, we use eight values of LAI: 0.1, 0.5, 1, 2, 3, 4, 5, and 6. Also, the pressure, the temperature, and the vapour pressure of the air surrounding the leaf used to compute the internal  $\text{CO}_2$  concentration of the leaf are set to 1000 hPa, 25 °C, and 10 hPa, respectively. The carbon dioxide ( $\text{CO}_2$ ) and the oxygen ( $\text{O}_2$ ) concentrations are set to 355 ppm and  $210 \times 10^3$  ppm, respectively. The other settings of SCOPE relevant for this study are given in Table 1.

- To investigate the sensitivity of SIF and GPP to the maximum carboxylation capacity  $V_{\text{cmax}}$ , we choose  $V_{\text{cmax}}$  values ranging from 10 to  $250 \mu\text{mol}(\text{CO}_2) \text{ m}^{-2} \text{ s}^{-1}$  every  $10 \mu\text{mol} \text{ m}^{-2} \text{ s}^{-1}$ . In addition, two small  $V_{\text{cmax}}$  values of 0.5 and  $5 \mu\text{mol} \text{ m}^{-2} \text{ s}^{-1}$  are considered.
- To study the sensitivity of SIF and GPP to the chlorophyll AB content ( $C_{\text{ab}}$ ), we select  $C_{\text{ab}}$  values that span 10 to  $80 \mu\text{g} \text{ cm}^{-2}$  range every  $5 \mu\text{g} \text{ cm}^{-2}$ . Additionally, a small  $C_{\text{ab}}$  value of  $1 \mu\text{g} \text{ cm}^{-2}$  is considered.
- To assess the sensitivity of the SIF and GPP to the broadband incoming shortwave radiation ( $0.4\text{--}2.5 \mu\text{m}$ ; hereafter  $R_{\text{in}}$ ) at the top of the canopy, we select  $R_{\text{in}}$  values that range from 100 to  $1200 \text{ W m}^{-2}$  every  $100 \text{ W m}^{-2}$ . We add small values of 1, 5, 10, 25, 50, and  $75 \text{ W m}^{-2}$ .
- Finally, to investigate the diurnal variations, we simulate SIF and GPP by using the short time series of half-hourly data over 15–20 July 2004 over a canopy located at the Hyttiala research site in Finland ( $61.85^\circ$

latitude and 24.29° longitude), which is one of the sites of the FLUXNET network (e.g., Baldocchi, 2003; Papale et al., 2006; see the dedicated website: <http://www.fluxnet.ornl.gov>). SCOPE GPPs are compared to the observationally derived GPP data. Unfortunately, we do not have observed SIF for this period.

### 3.2 CCDAS simulations

Since the idealized tests may give a partial picture of the relationship between SIF and GPP, we use the CCDAS built around SCOPE to perform additional sensitivity tests by using actual meteorological, radiation, and phenological data over 2009–2010. Overall, the values of the short wave radiation  $R_{in}$  used in the CCDAS are mostly under moderate light conditions (around 400–600  $W m^{-2}$ ), but at some pixels  $R_{in}$  values can be larger than 800  $W m^{-2}$  (see Sect. S3 in the Supplement). The relationship between SIF and GPP is then investigated along with  $V_{cmax}$  and  $C_{ab}$ . We make simulations of SIF and GPP by using prior values of  $V_{cmax}$  and their optimized values from Koffi et al. (2012). We also carry out simulations by using a constant value of  $C_{ab}$  for all the 13 PFTs and a set of  $C_{ab}$  values for each of them. We perform four experiments (i.e., S1 to S4), which are summarized in Table 3. The experiments S1 and S3 use a constant value of  $C_{ab}$  for all of the 13 PFTs, while simulations S2 and S4 consider  $C_{ab}$  to be PFT dependent ( $C_{ab}$  values are reported in Table 2). The experiments S1 and S2 consider the prior values of  $V_{cmax}$ , while S3 and S4 their optimized values. The differences between S1 and S3 or between S2 and S4 give the sensitivity of SIF and GPP to  $V_{cmax}$ . The differences between S1 and S2 or between S3 and S4 mainly give the sensitivity of SIF to  $C_{ab}$ .

The CCDAS simulates hourly SIF and GPP for one representative day in a month. Since the computation of fluorescence is time consuming, we compute both SIF and GPP only at 12 h local time, i.e., around the time of their peaks during a sunny day. For the simulated SIF, the computations are assigned to the 15th day of the month by using the monthly climate data and phenological variables of BETHY, as described in Sect. 2.2.2. We also neglect the energy balance scheme in SCOPE which weakly affects SIF.

## 4 Results

### 4.1 Idealized sensitivity tests using SCOPE

The results of these idealized sensitivity tests for the various LAI values are summarized in Figs. 2 and 3. For clarity, results from C3 plant are discussed. Then, some conclusions are given for C4 plant.

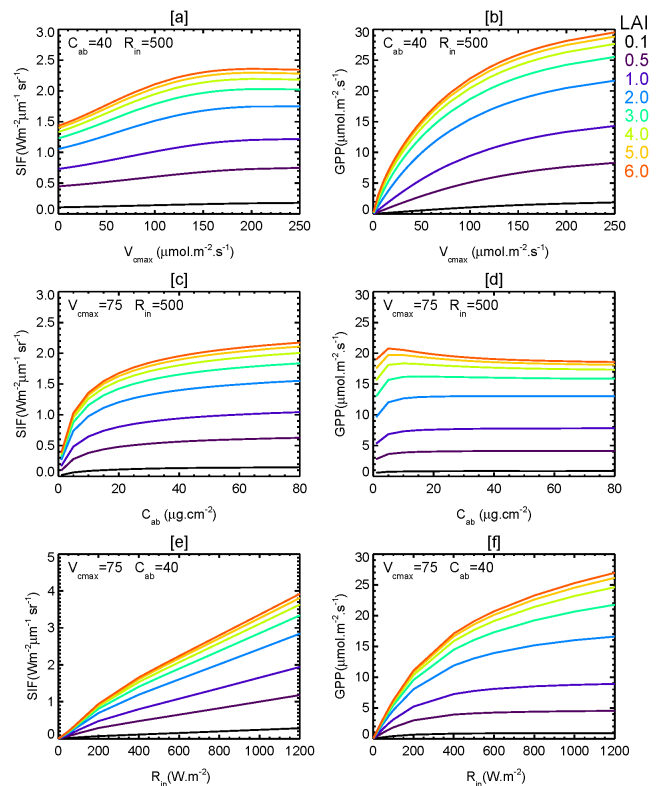


**Figure 2.** The sensitivities of SCOPE fluorescence (SIF) at the top of the canopy of C<sub>3</sub> plant to the carboxylation maximum capacity ( $V_{cmax}$ ), chlorophyll AB content ( $C_{ab}$ ), and to the broadband incoming shortwave radiation (0.4–2.5  $\mu m$ ) ( $R_{in}$ ) for several leaf area indices (LAI) are shown. Graphs (a) and (b) stand for SIF and GPP as function of  $V_{cmax}$ , respectively. Graphs (c) and (d) give the sensitivities of SIF and GPP to  $C_{ab}$ , respectively. Graphs (e) and (f) show SIF and GPP as a function of  $R_{in}$ , respectively.

#### 4.1.1 Sensitivity of SIF and GPP to biochemistry parameters

Figure 2 shows the sensitivity of both SIF and GPP to LAI,  $V_{cmax}$ , and  $C_{ab}$  under moderate light conditions ( $R_{in} = 500 W m^{-2}$ ). As expected, both the fluorescence SIF and GPP increase with the increase of LAI (Fig. 2). However, a weak sensitivity is found for LAI values greater than 4. As an illustration for the increase, for  $V_{cmax} = 50 \mu mol m^{-2} s^{-1}$ , SIF values of 0.5 and 1.25  $W m^{-2} \mu m^{-1} sr^{-1}$  are found for LAI of 0.5 and 2, respectively (Fig. 2a). The fluorescence slightly increases with an increase of  $V_{cmax}$ . The sensitivity is relatively large for  $V_{cmax}$ , less than 70  $\mu mol m^{-2} s^{-1}$ . Then, SIF remains almost constant for  $V_{cmax}$  higher than 125  $\mu mol m^{-2} s^{-1}$  (Fig. 2a). As an illustration, for LAI = 2, the largest increase is of only 50 % of SIF for  $V_{cmax}$  between 10 and 70  $\mu mol m^{-2} s^{-1}$ . Under the studied configurations SIF increases with  $V_{cmax}$  when the GPP is controlled by the carboxylation enzyme Rubisco, and remains almost constant when photosynthesis is limited by electron transport.

**Table 3.** Set-ups for the CCDAS simulations based on the carboxylation maximum capacity ( $V_{\text{cmax}}$ ) and chlorophyll AB content ( $C_{\text{ab}}$ ) are given. The values of prior and optimized  $V_{\text{cmax}}$  as well as  $C_{\text{ab}}$  PFT-specific are given in Table 2. The constant value of  $C_{\text{ab}}$  for all 13 PFTs is set to  $40 \mu\text{g cm}^{-2}$ .

Model configuration	$V_{\text{cmax}}$	$C_{\text{ab}}$
S1	Prior values	Constant value for all the 13 PFTs
S2	Prior values	$C_{\text{ab}}$ PFT-specific
S3	Optimized values	Constant value for all the 13 PFTs
S4	Optimized values	$C_{\text{ab}}$ PFT-specific

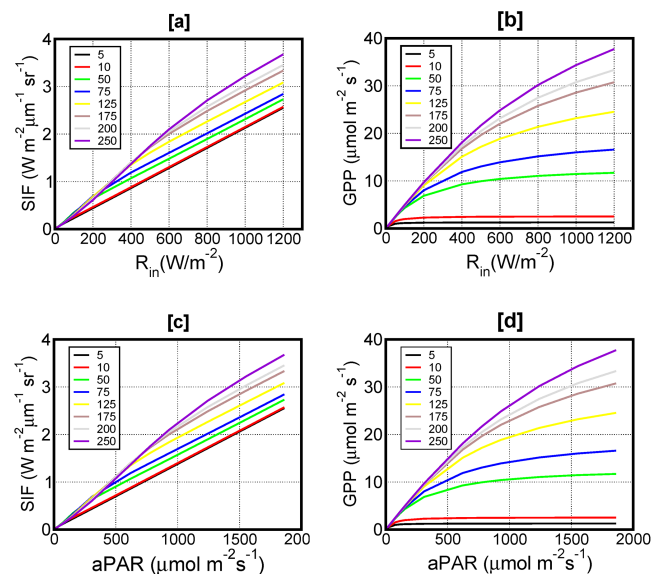


**Figure 3.** The sensitivities of the SCOPE fluorescence SIF (a and c) and gross primary productivity (GPP) (b and d) to the incoming short wave radiation ( $R_{\text{in}}$ ) and absorbed photosynthetically active radiation (aPAR) and for several  $V_{\text{cmax}}$  are presented. LAI and  $C_{\text{ab}}$  are set to 2 and  $40 \mu\text{g cm}^{-2}$ , respectively. Results for a  $C_3$  plant are shown.

GPP monotonically increases as  $V_{\text{cmax}}$  increases with large sensitivity for small  $V_{\text{cmax}}$  (less than  $75 \mu\text{mol m}^{-2} \text{s}^{-1}$ ), then it becomes weakly sensitive for large values of  $V_{\text{cmax}}$  (Fig. 2b). A moderate positive correlation is found between SIF and GPP for  $V_{\text{cmax}}$  less than  $125 \mu\text{mol m}^{-2} \text{s}^{-1}$ , as shown by the increase of both SIF and GPP with  $V_{\text{cmax}}$  (Fig. 2a and b). Then, for larger  $V_{\text{cmax}}$  (i.e.,  $125 \mu\text{mol m}^{-2} \text{s}^{-1}$ ), a very weak negative correlation between SIF and GPP is obtained. The reason for this weak negative correlation is that SIF slightly decreases for large  $V_{\text{cmax}}$ , while GPP even limited by the carboxylation enzyme Rubisco still slightly increases (Fig. 2a and b). In fact, the value of irradiance at which the fluorescence yield at leaf level  $\Phi_{\text{Ft}}$  (Eq. 1) or SIF peaks increases with the increase of  $V_{\text{cmax}}$ . Thus, for the case presented in Fig. 2a with the short wave radiation  $R_{\text{in}}$  of  $500 \text{W m}^{-2}$ , the peak of SIF occurs at about  $V_{\text{cmax}} = 200 \mu\text{mol m}^{-2} \text{s}^{-1}$ .

In the current version of the fluorescence model in SCOPE, the concentration of chlorophyll  $C_{\text{ab}}$  is set as a parameter and it is linked to SIF through the transmittance and reflectance of the leaves. Figure 2c portrays the variations of SIF as a function of  $C_{\text{ab}}$  and for various LAIs. For a given LAI, SIF increases with  $C_{\text{ab}}$  with large sensitivity for  $C_{\text{ab}}$  less than  $20 \mu\text{g cm}^{-2}$ . For larger  $C_{\text{ab}}$  values (i.e.,  $> 50 \mu\text{g cm}^{-2}$ ), SIF remains almost constant with a tendency to slightly decrease as  $C_{\text{ab}}$  increases. For a given  $C_{\text{ab}}$ , the variance in SIF due to the LAI can be significant.

Fig. 2d displays GPP as a function of  $C_{\text{ab}}$  (Fig. 2d). Except for small values of  $C_{\text{ab}}$  (less than  $5 \mu\text{g cm}^{-2}$ ), GPP is not sensitive to  $C_{\text{ab}}$ . The very weak sensitivity of GPP to  $C_{\text{ab}}$  comes from the impact of the chlorophyll content on the transmittance and reflectance at the top of the canopy when computing the aPAR. This lack of sensitivity of GPP to  $C_{\text{ab}}$  contradicts the established positive relationship between the two variables as reported in Fleischer (1935) and more recently in Gitelson et al. (2006).

#### 4.1.2 Sensitivity of SIF and GPP to short wave radiation

For a given LAI, both SIF and GPP increase with the top of canopy short wave radiation ( $R_{\text{in}}$ ) (Fig. 2e and f). Thus, a strong positive linear correlation is obtained between SIF and  $R_{\text{in}}$  (Fig. 2e), while a non-linear (i.e., curvilinear) relationship is obtained between GPP and  $R_{\text{in}}$  (Fig. 2f). For large  $R_{\text{in}}$ , GPP increases with a slower rate indicating that the photosynthesis is limited by the carboxylation enzyme Rubisco. For the selected values of LAI, large variance is found between SIF and  $R_{\text{in}}$  (Fig. 2e). We also investigate the relationship between the simulated aPAR and both computed SIF and GPP (see Sect. S1 in the Supplement). As expected, a very strong linear relationship between SIF and aPAR is obtained. This relationship is less sensitive to the LAI as it is for the relation between SIF and  $R_{\text{in}}$  (as shown in Fig. 2e). GPP shows similar variations with aPAR as it does with the short wave radiation in Fig. 2f.

Finally, the sensitivities of SIF and GPP to both  $R_{\text{in}}$  and aPAR for various  $V_{\text{cmax}}$  are also investigated (Fig. 3). A strong linear relationship between SIF and both  $R_{\text{in}}$  and aPAR is obtained with slopes which are less sensitive to the values of  $V_{\text{cmax}}$  (Fig. 3a and c). Also, results clearly show

that the sensitivity of SIF to  $V_{\text{cmax}}$  increases with the increase of aPAR (or  $R_{\text{in}}$ ), with almost no sensitivity for low values of aPAR ( $< 250 \mu\text{mol m}^{-2} \text{s}^{-1}$ ). However, even with large values of aPAR (or  $R_{\text{in}}$ ), the sensitivity of SIF to  $V_{\text{cmax}}$  remains small. In fact, the sensitivity of SIF to  $V_{\text{cmax}}$  slightly increases with increasing of incoming radiation only when  $V_{\text{cmax}}$  rapidly increases from low to high values (e.g. 5 to  $250 \mu\text{mol m}^{-2} \text{s}^{-1}$ ; Fig. 3a and c). Such a rapid increase of  $V_{\text{cmax}}$  does occur only during the growing season of the plant. As expected, a curvilinear relationship is found between GPP and both  $R_{\text{in}}$  and aPAR with large variance in this relation for the selected  $V_{\text{cmax}}$  (Fig. 3b and d).

It is worth noting that SIF values present in Fig. 3 in this study differ (here lower) from the fluorescence flux at leaf level shown in van der Tol et al. (2014). In fact, the authors argued that in the canopy, leaf illumination is variable among leaves, and the relationship after aggregating over all leaves (i.e., SIF) may differ from the fluorescence flux at leaf level.

The conclusions found from C3 plant relevant for the sensitivity of both SIF and GPP to the input variables ( $V_{\text{cmax}}$ ,  $C_{\text{ab}}$ , and  $R_{\text{in}}$ ) are valid for C4 plant (see Sect. S1). However, the amplitude of these sensitivities is slightly larger for C4 plant.

#### 4.1.3 Simulations of in situ measurements

The time series of both simulated SIF and GPP for 15–20 July 2004 are presented in Fig. 4. As expected, there is a strong correlation between aPAR and the short wave radiation  $R_{\text{in}}$  (Fig. 4b), hence we discuss the results as a function of the observed  $R_{\text{in}}$ . The temporal variations of SIF and GPP mainly follow that of  $R_{\text{in}}$ . Particularly, the variations of SIF mirror that of  $R_{\text{in}}$ , showing that the variance in SIF due to the temperature is low in this case study (Fig. 4a). At high irradiance GPP shows limitation by the carboxylation enzyme Rubisco, peaking early in the day whereas SIF follows  $R_{\text{in}}$  throughout the day. The small variations in GPP at certain episodes can be explained by the temporal variations of the temperature (Fig. 4a). Note that  $V_{\text{cmax}}$ ,  $C_{\text{ab}}$ , and LAI are set constant during this period. Consequently, for this case study, the short wave radiation (hence aPAR) is the main driver of the relationship between simulated SIF and GPP. A curvilinear relation is obtained between GPP and SIF. However, a relatively strong linear correlation coefficient of 0.95 is derived. This suggests that SIF is a good constraint of GPP even if it does not directly constrain  $V_{\text{cmax}}$ . The SCOPE model reproduces the observed diurnal GPP quite well with meaningful choices of both LAI and  $V_{\text{cmax}}$  values (Fig. 4d). Again, the simulated SIF is sensitive to  $C_{\text{ab}}$ , while GPP is insensitive to  $C_{\text{ab}}$  (Figs. 4c and d).

Furthermore, we have computed the seasonal variations of these quantities for some years at Hyytiälä and Roccarespampani1 (acronym IT-Ro1, longitude/latitude of 11.93/42.408) (see Sect. S2 in the Supplement). Overall, the model reproduces quite well the observed GPP. However, the simu-

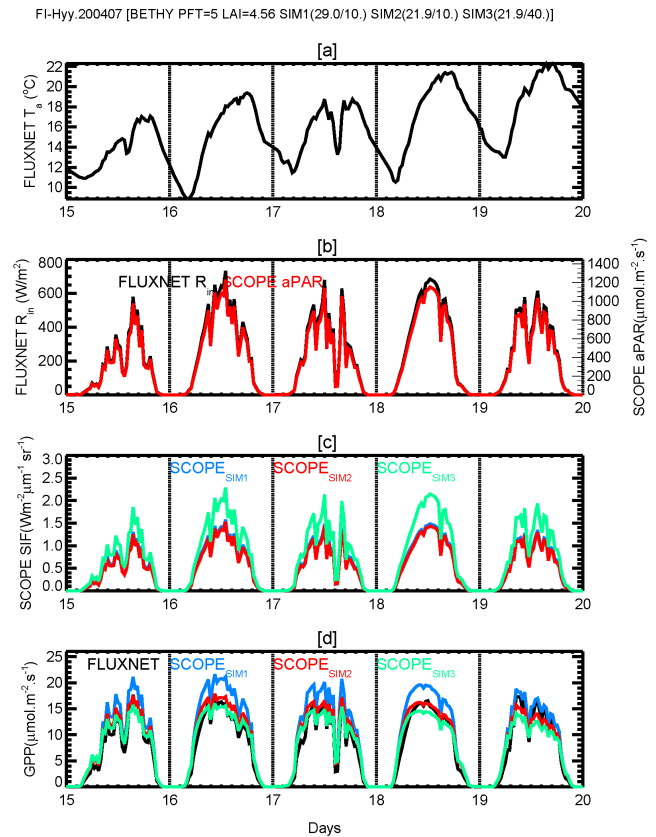


**Figure 4.** SCOPE simulations of fluorescence SIF, gross primary productivity (GPP), and absorbed photosynthetically active radiation (aPAR) from in situ measurements at Hyytiälä (acronym FI-Hyy and having longitude/latitude of  $24.295^{\circ} \text{E}/61.847^{\circ} \text{N}$ ) in Finland during 2004 over the 15 July to 20 July period. Graph (a) presents the temporal variations of the observed temperature ( $T_{\text{a}}$ ). Graph (b) shows the temporal variations of both observed incoming short wave radiation  $R_{\text{in}}$  (black) and SCOPE simulated aPAR (red). Graphs (c) (SIF) and (d) (GPP) present SCOPE simulations by using two values of both  $V_{\text{cmax}}$  and  $C_{\text{ab}}$  (blue: SCOPE<sub>SIM1</sub>:  $V_{\text{cmax}}/C_{\text{ab}} = 29 \mu\text{mol m}^{-2} \text{s}^{-1}/10 \mu\text{g cm}^{-2}$ ; red: SCOPE<sub>SIM2</sub>: 21.91/10.; green SCOPE<sub>SIM3</sub>: 21.91/40). The observed GPP is in black. The other SCOPE parameters are given in Table 1. The C3 plant is considered in SCOPE simulations.

lated SCOPE GPP peak over a year occurs earlier (within 1–2 months) than observed ones. This result is maybe caused by both LAI and  $V_{\text{cmax}}$  used for the simulation, which seem apparently large during the growing season of the vegetation at these sites. The results of these preliminary analyses can be then reinforced by using e.g., the satellite MODIS weekly LAI data relevant for these stations.

In summary, these idealized tests clearly show that the fluorescence SIF is more sensitive to  $C_{\text{ab}}$ , while GPP is more sensitive to  $V_{\text{cmax}}$  and both quantities are strongly sensitive to the short wave radiation (or aPAR). However, GPP is limited by the carboxylation enzyme Rubisco for large values of short wave radiation (or aPAR). Consequently, in this case

the relationship between SIF and GPP mainly driven by the short wave radiation (or aPAR) is curvilinear. The part of the variance in this relationship due to the GPP can be explained by  $V_{\text{cmax}}$  and environment conditions, while the variance in SIF is mainly due to  $C_{\text{ab}}$  and possibly to the geometrical parameters (i.e., solar zenith angle and observation zenith angle) used in the retrieval of SIF.

Recent investigations by Zhang et al. (2014) show a strong sensitivity of SIF to  $V_{\text{cmax}}$  at in situ level at light saturation for cropland (corn and soybean) using SCOPE version 1.52. Zhang et al. (2014) found about 4 times our sensitivity of SIF (here computed at 755 nm; Fig. 3a) to  $V_{\text{cmax}}$  in the range of 10–200  $\mu\text{mol m}^{-2} \text{s}^{-1}$ . We have modified our experiments to bring them closer to those of Zhang et al. (2014). First, Zhang et al. (2014) calculate SIF at 740 nm vs. 755 nm in this study. Secondly, Zhang et al. (2014) average their calculations from 9:00–12:00 local time (LT), while we sample at 12:00 LT. Results show that:

- The sensitivity of SIF to  $V_{\text{cmax}}$  is slightly larger at 740 than 755 nm and the difference increases with aPAR. However, as an example, for a relatively large aPAR (1400  $\mu\text{mol m}^{-2} \text{s}^{-1}$ ), SIF at 740 nm is only 25 % higher than SIF at 755 nm.
- The averaging period makes little difference to the sensitivity.
- Optimal choices of temperature and LAI produce a sensitivity about 2/3 that shown in Zhang et al. (2014). Details on these comparisons are given in the Supplement (Sect. S4).

## 4.2 CCDAS simulations

To assess the relationship between SIF and GPP at global scale, we perform CCDAS simulations for the four experiments described in Table 3. The observed (SIF) and modelled (SIF, GPP, and aPAR) quantities are generated at monthly time resolution as described in Sects. 2.2.1 and 3.1, respectively. The results of these simulations are discussed along with the satellite-based SIF. We first analyze the correlations between the simulated quantities and also the correlations between these simulations and the satellite-based SIF. Secondly, their mean spatial patterns are discussed and finally, the time series of their global and regional means as well as their zonal averages are discussed.

### 4.2.1 Correlations between SIF and GPP

For the discussion of the time series of modelled SIF and GPP at each CCDAS land pixel and the corresponding observed SIF we analyze only pixels for which we have at least 1 year satellite-based SIF data. Moreover, we consider only the time series of these quantities for which the satellite-based SIF data show consecutive values equal or greater than zero. Indeed, the SCOPE model does not allow simulating

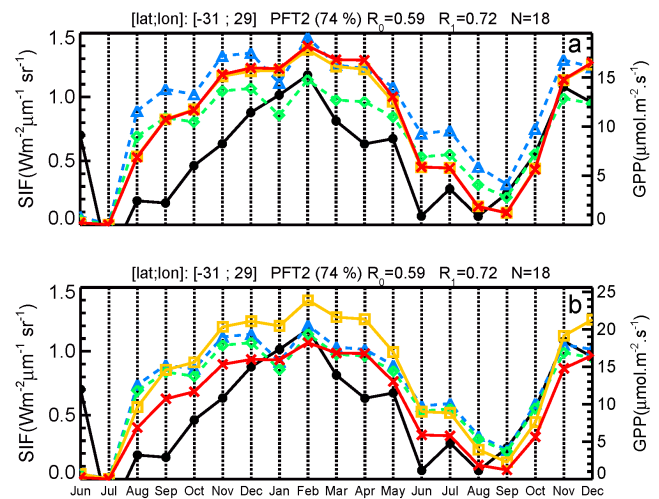


**Figure 5.** Temporal variations (June 2009 to December 2010) of CCDAS simulations of the fluorescence SIF and GPP for different values of the carboxylation maximum capacity ( $V_{\text{cmax}}$ ) and the chlorophyll AB content ( $C_{\text{ab}}$ ) and for (a) plant functional type (PFT 2: Tropical broadleaved evergreen tree) are shown. In both graphs (a and b), the satellite GOSAT based SIF is shown in black solid line with big dots.

In graph (a), SIF and GPP are simulated by using  $V_{\text{cmax}}$  value of 73.5  $\mu\text{mol}(\text{CO}_2) \text{m}^{-2} \text{s}^{-1}$  and two  $C_{\text{ab}}$  values of 40  $\mu\text{g cm}^{-2}$  (SIF in blue dashed line with triangles and GPP in red solid line with crosses) and 15  $\mu\text{g cm}^{-2}$  (SIF in green dashed line with diamond and GPP in orange solid line with rectangles), respectively. For  $C_{\text{ab}}$  value of 15  $\mu\text{g cm}^{-2}$ , the correlation coefficient  $R_0$  between simulated SIF and satellite based SIF is given on the top of the graph.

In graph (b), SIF and GPP are simulated by using  $C_{\text{ab}}$  value of 15  $\mu\text{g cm}^{-2}$  and two  $V_{\text{cmax}}$  values of 90  $\mu\text{mol}(\text{CO}_2) \text{m}^{-2} \text{s}^{-1}$  (SIF in blue dashed line with triangles and GPP in orange solid line with rectangles) and 73.5  $\mu\text{mol}(\text{CO}_2) \text{m}^{-2} \text{s}^{-1}$  (SIF in green dashed line with diamonds and GPP in red solid line with crosses), respectively. For  $V_{\text{cmax}}$  value of 73.5  $\mu\text{mol}(\text{CO}_2) \text{m}^{-2} \text{s}^{-1}$ , the correlation coefficient  $R_1$  between simulated GPP and satellite based SIF is given on the top of the graph.

negative SIF values. Overall, the seasonality of the satellite-derived SIF is reasonably well reproduced by both the simulated SIF and GPP as illustrated in Fig. 5. In accordance with the idealized tests, the amplitudes of the satellite-derived SIF can be better fitted by appropriate values of  $C_{\text{ab}}$  (Fig. 5a), while the simulated GPP is only weakly sensitive to small  $C_{\text{ab}}$  values as discussed in Sect. 4.1. As expected, the amplitudes of the simulated GPP are strongly sensitive to  $V_{\text{cmax}}$  (Fig. 5b).

We have computed the Pearson correlation coefficient between the time series of satellite-based SIF and modelled SIF and GPP at each pixel. For each pixel, we consider only the pair of data for which the satellite-based SIF is greater than or equal to zero. At most, 18 pairs of data are available for each pixel. We treat only pixels with at least 14 data points for which the linear correlation is significant at least 10 % of

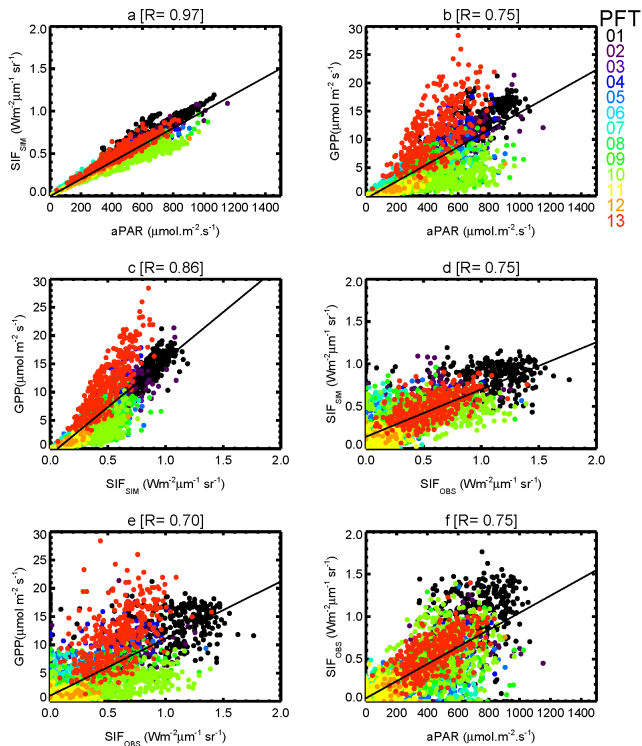


**Figure 6.** Correlations between CCDAS simulated quantities (i.e., SIF, GPP, aPAR) and between these simulated quantities and satellite GOSAT based fluorescence SIF are shown. Graph (a) presents the correlation between CCDAS simulated SIF ( $SIF_{SIM}$ ) and the simulated absorbed photosynthetically active radiation (aPAR). Graph (b) shows the simulated gross primary productivity (GPP) as function of aPAR. Graph (c) displays the scatter plot between simulated GPP and simulated SIF. Graph (d) presents the correlation between  $SIF_{SIM}$  and  $SIF_{OBS}$ . Graph (e) displays simulated GPP as function of  $SIF_{OBS}$ . Graph (f) shows  $SIF_{OBS}$  as a function of aPAR. The dominant plant functional types (PFT) in the grid cell, characterized by the PFTs having at least 50 % of the spatial coverage, are shown by different colours on the right hand side of graph (b). The pixels of the CCDAS are at the spatial resolution of  $2^\circ \times 2^\circ$  (longitude  $\times$  latitude). Results at global scale are shown. The number of pair of data is 2857. The Pearson coefficient of the linear correlation  $R$  is indicated. Data for June 2009 to December 2010 period are considered.

level of significance for Pearson coefficient  $R$  greater than 0.43. For about half of the 3462 land pixels of CCDAS, the linear correlation coefficient  $R$  between the satellite-based SIF and either simulated SIF or GPP is less than 0.43. For these latter pixels, we have analyzed the time series of the satellite-based SIF (with their uncertainty) jointly with the simulated SIF and GPP together with the aPAR as representative of the short wave radiation. For brevity sake, we only enumerate the different cases with low correlation (i.e.,  $R < 0.43$ ) without quantification since this does not add anything valuable to our demonstration in the current study. We have cases for which:

- The peaks in simulated quantities (i.e., SIF and GPP) lag the satellite-based SIF peak by at least 1 month. Other cases show opposite behaviour.
- The simulated SIF remain almost constant, while the satellite-based SIF show a weak seasonality. Such cases predominantly occur in the tropics.
- The satellite-based SIF are larger ( $> 2 \text{ Wm}^{-2} \mu\text{m}^{-1} \text{sr}^{-1}$ ) than modelled SIF (around  $1.2 \text{ Wm}^{-2} \mu\text{m}^{-1} \text{sr}^{-1}$ ). Such cases are mainly obtained in the tropics and for the PFT 1 (i.e., tropical broadleaved evergreen tree).
- The simulated SIF are larger than satellite based SIF. Such cases are mainly obtained from the PFT 9 (i.e., C3 grass).
- The satellite-based SIF show some unexpected peaks during period where they are not expected and hence not modelled.

Secondly, we investigate the correlations between the simulated quantities (SIF, GPP, and aPAR) at regional scales by using our best set up (i.e., experiment S4 in Table 3). We then assess the correlations between the simulated quantities (SIF, GPP, and aPAR) and between simulated quantities and the satellite-based SIF. We select data at each pixel such that the satellite-based SIF is greater or equal to zero and CCDAS land pixel (i.e., the maximum fraction of coverage of the dominant PFT of the pixel) is greater than zero. Data from June 2009 to end of 2010 are analyzed. We also give information about the dominant PFT of the pixels over the studied time period. To sample only over grid cells which are dominated by only one PFT, we consider only pixels for which the dominant PFT has a fraction of coverage greater than 50 %. Correlations are computed at global and regional (southern hemisphere, tropics, and southern hemisphere) scales and over the studied period. The results at global scale are shown in Fig. 6. A strong linear correlation is found between the computed SIF and aPAR. This relation is weakly sensitive to the PFTs (Fig. 6a). In contrast, the relationship between GPP and aPAR is PFT dependent (Fig. 6b). A good linear relationship between computed GPP and simulated SIF is obtained and again the slopes of this relationship are PFT dependent (Fig. 6c). The correlation coefficient  $R$  derived from GPP as a function of SIF value is around 0.8.

The model SCOPE simulates quite well the observed SIF (Fig. 6d). However, large observed SIF ( $> 2 \text{ Wm}^{-2} \mu\text{m}^{-1} \text{sr}^{-1}$ ) are not simulated. Such large observed SIF mainly occur in the tropics. This result points out that short wave radiation used in the CCDAS simulations may be smaller than actual values. Also, the parameter  $K_n$  (Eq. 3) in the SCOPE model may explain part of these low SIF. In fact, the computation of the fluorescence yield  $\Phi_{Fm}$  (Eq. 2) depends on the parameter  $K_n$ , which is unknown and there is no theoretical basis to constrain it. Thus, an empirical relationship of  $K_n$  is used to calculate  $\Phi_{Fm}$ . In the current

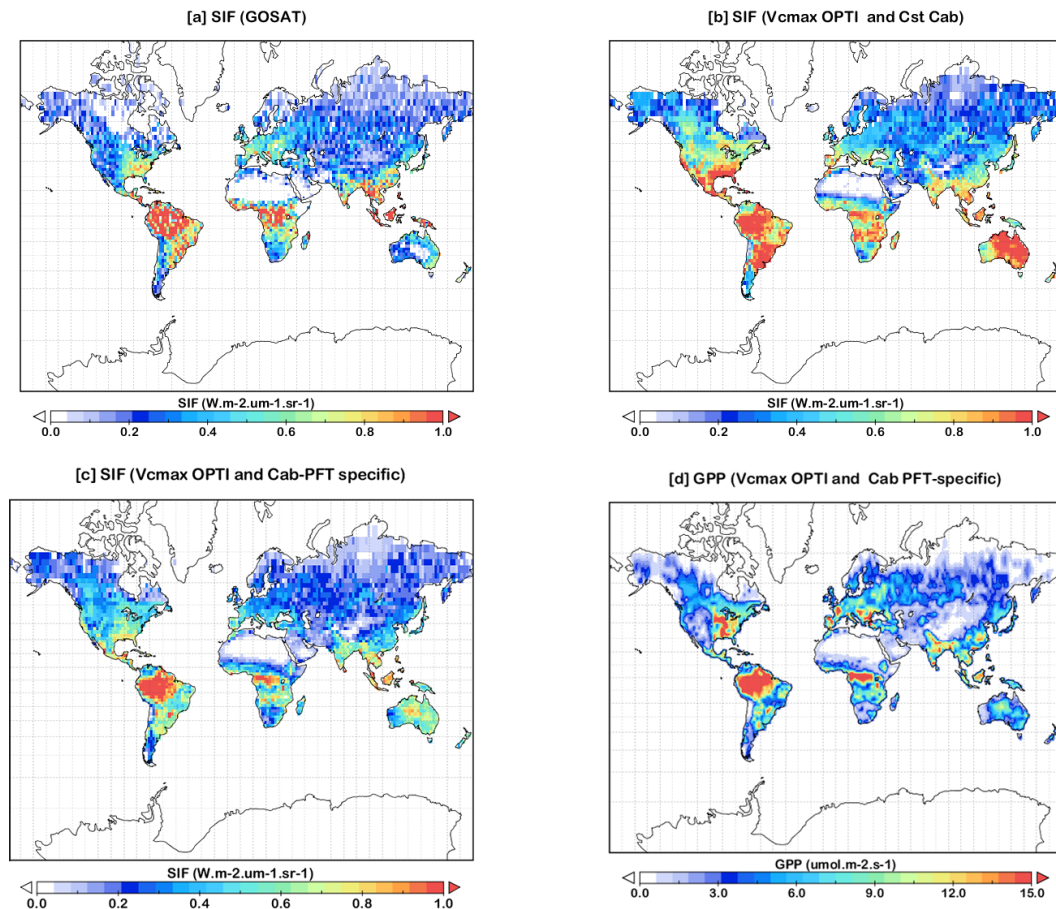


**Figure 7.** Mean spatial patterns over the year 2010 of (a) satellite GOSAT based fluorescence SIF, (b) CCDAS simulated SIF by using constant value of the chlorophyll AB content ( $C_{ab}$ ) for all the 13 PFTs (setting S3 in Table 3), (c)  $C_{ab}$  PFT specific (setting S4 in Table 3) are shown. Graph d) displays the mean spatial patterns of the gross primary productivity (GPP) by using both  $C_{ab}$  PFT specific and optimized carboxylation maximum capacity ( $V_{cmax}$ ) (setting S4 in Table 3).

version of the model SCOPE, there are two parametrizations of  $K_n$ . In this paper, we use the parameterization of  $K_n$  from Flexas et al. (2002)'s data set that includes drought stress (see Eq. 3). Nevertheless, we have tested the other parameterization and large differences are found from their SIF output. The contribution of chlorophyll content  $C_{ab}$  is low since the assigned value in tropics is already large ( $40 \mu\text{g cm}^{-2}$ ) and as shown by the idealized tests, the simulated fluorescence SIF remains almost constant for  $C_{ab}$  value larger or equal to  $40 \mu\text{g cm}^{-2}$  (Fig. 2c). The correlation coefficient between modelled GPP and satellite-based SIF is 0.70. This rises to 0.8 when we aggregate both quantities to  $4 \times 4$  degrees in agreement with Frankenberg et al. (2011). Finally, as expected, a relatively good correlation is found between aPAR and satellite-based SIF (Fig. 6f).

Correlations are found to be larger between simulated quantities and satellite-derived SIF in the northern hemisphere and moderate in the tropics and lower in the southern hemisphere (not shown).

#### 4.2.2 Mean spatial patterns of SIF and GPP

We compute the mean annual patterns of the satellite-based SIF and simulated SIF and GPP for 2010. We discuss the simulated quantities by using the experiments S3 (i.e., optimized  $V_{cmax}$  and constant  $C_{ab}$  for all the 13 PFTs) and S4 (optimized  $V_{cmax}$  and  $C_{ab}$  PTF-specific) (See Table 3).

Figure 7 displays the annual mean observed and simulated SIF as well as simulated GPP. Figure 7a shows the satellite-based SIF. Figure 7b displays the modelled SIF by using constant  $C_{ab}$  for the 13 PFTs (experiment S3; Table 3), while Fig. 7c presents model results of SIF for  $C_{ab}$  PTF-specific (experiment S4). Figure 7d exhibits the simulated GPP by using both  $C_{ab}$  PTF-specific and optimized  $V_{cmax}$  (experiment S4). The model can reasonably reproduce the mean spatial patterns of the satellite-based SIF with an appropriate choice of  $C_{ab}$  values for each of the 13 PFTs (Fig. 7a and c). The model with constant  $C_{ab}$  cannot reproduce the locations of maximum observed SIF (Fig. 7a and b). Despite the good correlation, the computed SIF with PFT-specific  $C_{ab}$

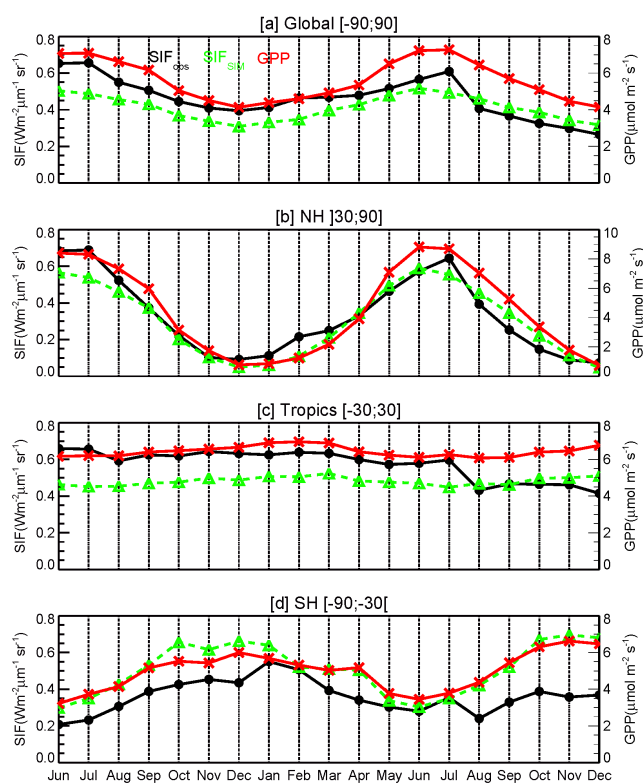


**Figure 8.** Global (a) and regional (b to d) means of fluorescence SIF and gross primary productivity GPP over June 2009 to December 2010 period are shown. The satellite GOSAT based SIF ( $SIF_{OBS}$ : black solid line with big dot), simulated SIF ( $SIF_{SIM}$ : green dashed line with triangles), and the simulated gross primary productivity (GPP: red solid line with crosses) are displayed. The CCDAS set up S4 (Table 3) is considered.

(Table 3) underestimates the satellite-based data (Fig. 7a and c). Some of this mismatch corresponds to unlikely simulated SIF, for example, in central Australia.

A good agreement between the spatial patterns of GPP and satellite-based SIF is found (Fig. 7a and d). Overall, we have a co-occurrence of hot spots of observed SIF and simulated SIF and GPP. Moreover, maximum simulated SIF coincides with maximum aPAR (not shown).

The small sensitivity of simulated SIF to  $V_{cmax}$  suggests that it may be difficult to use observations of SIF to constrain it. We can test this in a more realistic context by comparing the differences between simulated SIF for prior and optimized values of  $V_{cmax}$ . If differences are large compared to uncertainties in the observation then SIF observations would allow constraining  $V_{cmax}$ . We compute the differences between simulated SIF by using prior  $V_{cmax}$  (experiment S2 in Table 3) and optimized  $V_{cmax}$  (experiment S4). Then, we normalize these differences by the uncertainties in satellite-based SIF. The derived root mean square over the year 2010 at pixel level can reach up to 67% of the observed uncertainties, but the global average is only 6%. This suggests that

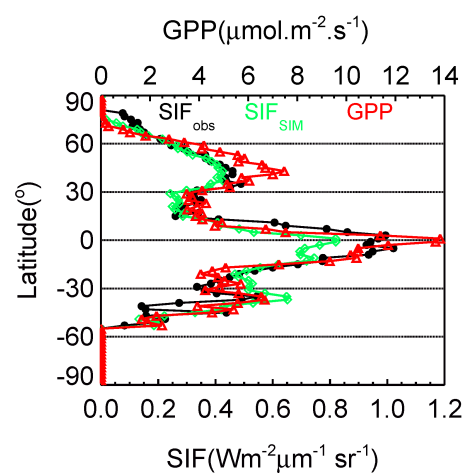


**Figure 9.** Latitudinal distributions of the satellite GOSAT based SIF ( $SIF_{OBS}$ : black solid line with big dot), simulated SIF ( $SIF_{SIM}$ : green solid line with diamonds), and gross primary productivity (GPP: red solid line with triangles) within  $5^\circ$  latitudinal band are shown. The CCDAS set up S4 (Table 3) is considered. The period of June 2009 and December 2010 period is considered.

SIF measurements can only weakly constrain  $V_{cmax}$  within the current CCDAS.

#### 4.2.3 Global and regional means of SIF and GPP

We compute the global and regional (i.e., Northern hemisphere [ $30^\circ N$ – $90^\circ N$ ] Tropics [ $30^\circ S$ – $30^\circ N$ ] and Southern hemisphere [ $90^\circ S$ – $30^\circ S$ ]) means at each month of the year and over June 2009 to December 2010 over land pixels. Results of both simulated SIF and GPP from our best experimental set up (i.e., optimized  $V_{cmax}$  with  $C_{ab}$  PTF-specific; experiment S4 in Table 3) are discussed. The results show a reasonably good agreement between satellite-based SIF and both simulated SIF and GPP in terms of seasonality (Fig. 8). However, on average, the simulated quantities peak 1 month earlier than the peak of the satellite-based SIF (Fig. 8a). In the Northern hemisphere, satellite-based SIF peaks in July, while simulated SIF reaches its maximum in June (Fig. 8b). The seasonality at global scale is dominated by the Northern hemisphere (Fig. 8a and b). In the Tropics, there is no significant seasonality in the satellite-based SIF, which is also reproduced by the model (Fig. 8c). In the Southern hemisphere, the satellite-based SIF peaks in January, while modelled peaks in December (Fig. 8d). This weak seasonality shift in the CCDAS simulations is driven by the visible radiation at the top of the canopy (or aPAR) and LAI.

Quantitatively, the mean values of the simulated SIF are slightly smaller than that of satellite-based (about 93%) in the Northern hemisphere and the Tropics. Since the above-mentioned regions dominated the amplitude of SIF, a good agreement between simulated and satellite-based SIF is consequently found at global scale. The simulated SIF in

the Southern hemisphere is about 1.47 times the value of satellite-based SIF. The main differences occur in Australia where the relatively large values of modelled SIF are not shown in the satellite-based SIF data (see Fig. 7a and c).

The zonal averages over the CCDAS land pixels of the satellite-based SIF and the simulated quantities (SIF and GPP) are shown in Fig. 9. A good agreement is found between the latitudinal variations of the satellite-based SIF and the simulated SIF by using the  $C_{ab}$  PFT-specific (Fig. 9). Also, a good agreement is obtained between the satellite-based SIF and the GPP (Fig. 9) and between SIF and aPAR (see Sect. S3 in the Supplement). All of these quantities show maxima in the tropics and around 45° N. Simulated SIF values are smaller than the satellite-based SIF in the tropics. Between -15° and -45°, the differences are mainly due to C4 grass for which both the model's  $V_{cmax}$  and  $C_{ab}$  are apparently small. Around -35° latitude, the differences are mainly due to the fact that the model simulates a large SIF signal over Australia, while the satellite-based SIF shows only a small SIF signal. This discrepancy might be explained by the uncertainty in the LAIs set to the evergreen shrub in the CCDAS in this area. Apparently, the LAIs in the CCDAS seem larger than expected values that give satellite based SIF measurements.

In summary, the agreement between simulated and observed SIF is better as we move to larger and larger scales.

## 5 Discussion and concluding remarks

The first global maps of SIF retrieved from GOSAT measurements show promise in estimating the terrestrial gross photosynthetic uptake flux of CO<sub>2</sub> (GPP) (Frankenberg et al., 2011; Joiner et al., 2011). We have investigated the usefulness of these data in constraining GPP in the framework of CCDAS. We have augmented CCDAS with SCOPE, which allows the calculation of GPP and SIF at leaf and canopy level. In CCDAS, the relationship between SIF and GPP is mediated by process parameters, principally the maximum carboxylation capacity ( $V_{cmax}$ ). Parameters not currently included in CCDAS such as the chlorophyll content ( $C_{ab}$ ) of the leaves also affects the observed fluorescence and so constitutes a nuisance variable in an assimilation of SIF into CCDAS. We first calculate the sensitivity of SIF and GPP in the stand alone SCOPE model to a series of parameters, inputs or nuisance variables. SIF and GPP both respond strongly to incoming radiation suggesting that, insofar as this input is uncertain, SIF can provide a useful constraint. This uncertainty is currently not considered in the CCDAS under study.

The relationship between  $V_{cmax}$  and SIF is more complicated and weaker suggesting that the CCDAS approach of using model parameters to mediate information from SIF to GPP is unlikely to work.  $C_{ab}$  also controls SIF while it has little impact on the desired GPP making it a classical nuisance variable. Hence, in the relationship between simulated

SIF and GPP, part of the variance is due to  $C_{ab}$ . This study also shows that the use of SIF measurements in the model should account for chlorophyll concentration.

The simulations of CCDAS confirm the results from the idealized tests. Thus, the relationship between the simulated GPP and computed SIF is again found to be mainly controlled by the short wave radiation or aPAR. The analyses also show that a robust linear relationship between SIF and GPP can be inferred for each PFT. This result is in agreement with the findings of Guanter et al. (2012) and Parazoo et al. (2014).

We compared observed SIF with simulated SIF and GPP at global scale within the CCDAS. The analyses showed a need to select meaningful values for the chlorophyll content  $C_{ab}$  for each of the 13 PFTs to better reproduce the satellite-based SIF. The use of PFT-specific  $C_{ab}$  allows a better reproduction of the satellite-based SIF, with good co-location of the hot spots. Timing of large-scale means is also good but this breaks down at pixel level. The global and regional as well as the zonal averages of the simulated quantities (SIF and GPP) are in good agreement with the satellite-based SIF. On average, the peaks in simulated SIF and GPP lag by 1 month the peaks in satellite-derived SIF in both Southern and Northern hemispheres. The simulated quantities are found to be better correlated to the satellite-based SIF when integrating the data at global and regional scales. More particularly, we found a significant linear correlation between simulated GPP and observed SIF, but a large scatter within the data is obtained. Such a variance can be attributed partly to the type of vegetation (Guanter et al., 2012; Parazoo et al., 2014). Also, part of this variance is caused by both  $V_{cmax}$  and  $C_{ab}$ . Indeed, simulated GPP is more sensitive to  $V_{cmax}$ , while simulated SIF is sensitive to  $C_{ab}$ .

The study suggests some prospects for the use of satellite-based SIF to constrain GPP. While we found a good correlation between the global and regional and zonal averages of simulated quantities and satellite-based SIF, we do not find a common process parameter that propagates the information from the fluorescence to the GPP. Indeed, the relationship between GPP and satellite-based SIF is mainly driven by the short wave radiation or aPAR. Consequently, the mechanistic formulations of both SIF and GPP under study do not allow us to constrain GPP through  $V_{cmax}$ .

On the other hand, the results clearly show the good correlation between aPAR and both the fluorescence SIF and GPP, which support previous investigations. This both points to a simpler application of SIF in constraining GPP and a problem with the foregoing study. aPAR is an external forcing for the biochemical modules of the biosphere model (e.g., SCOPE or BETHY) which is taken to be well known. Errors in forcing (like other nonparametric errors) are added to the observational error in CCDAS (Rayner et al., 2005), but the observations are unable to improve estimates of forcing. The parametric studies above hence miss a potential role of the

SIF measurements in constraining GPP even if they cannot constrain process parameters.

Monteith (1972) proposed an empirical linear relation between GPP and aPAR which has been widely used by the satellite community to derive the GPP. The slope of this relationship is the efficiency ( $\epsilon_p$ ) with which the absorbed radiation is converted to fixed carbon.  $\epsilon_p$  varies with physiological stress. We have seen a good linear relationship between the fluorescence SIF and aPAR. Thus, the GPP is directly linked to SIF by the ratio  $\epsilon_p / \epsilon_f$ . Such an approach is described in a recent report of Berry et al. (2013). Moreover, Yang et al. (2015), when investigating a temperate deciduous forest, found that SIF incorporated information about both aPAR and light use efficiency (LUE), the two main components of GPP. The empirical approach would be easier to implement. It could be combined with other pertinent data for GPP (e.g., CO<sub>2</sub> or Carbonyl sulfide (COS) concentration) within a simplified CCDAS. This approach will be applied in a future study.

This study also shows a very weak sensitivity of GPP to the chlorophyll content ( $C_{ab}$ ) which is obtained for only small  $C_{ab}$ . This model result contradicts the established positive relationship between the two variables as reported in Fleischer (1935) and more recently in Gitelson et al. (2006). In the current version of the SCOPE model,  $C_{ab}$  and  $V_{cmax}$  are independent parameters, but in reality they are correlated. In fact,  $C_{ab}$  is related to the nitrogen content of the leaf which itself is linked to  $V_{cmax}$  (e.g., Kattge et al., 2009; Houborg et al., 2013). In addition, the nitrogen content of the leaf affects both the leaf transmittance and reflectance which influences the aPAR and then the GPP. Thus, through the inclusion of a nitrogen scheme a more apparent link between  $C_{ab}$  and GPP and greater sensitivity could be achieved.

As the SCOPE model development, as stated in van der Tol et al. (2014), the computation of the fluorescence yield  $\Phi_{Fm}$  (Eq. 2 in this paper) depend on the parameter  $K_n$ , which is unknown and there is no theoretical basis to constrain it. Thus, an empirical relationship of  $K_n$  is used to change  $\Phi_{Fm}$ . In the current version of the model SCOPE, there are two parametrizations of  $K_n$ . In this paper, we use the parameterization of  $K_n$  from a Flexas' data set that includes drought stress, as noted within the model. Nevertheless, we have tested the other parameterization and large differences are found from their SIF output. Consequently, more research is needed to consolidate SIF modelling in SCOPE biochemistry model as there can be a notable effect of different models for  $K_n$  on the photosystem yields and subsequent sensitivity of SIF.

Finally, in this study we have investigated the sensitivity of simulated SIF to  $V_{cmax}$  at the frequency of 755 nm. Other frequencies in the fluorescence spectrum need to be checked.

## 6 Conclusions

We have investigated the usefulness of satellite-derived fluorescence data to constrain GPP within CCDAS. We have coupled the SCOPE model to CCDAS to allow for the computing of both fluorescence SIF and GPP. We have assessed the sensitivity of both SIF and GPP to the environmental conditions at the interface of the canopy (short wave radiation and meteorological variables) and the biophysical parameters ( $V_{cmax}$  and  $C_{ab}$ ) by using idealized and CCDAS simulations. Our results show:

- As expected, GPP is strongly sensitive to  $V_{cmax}$ , while SIF is more sensitive to  $C_{ab}$  and only weakly sensitive to  $V_{cmax}$  under high radiation conditions and lower  $V_{cmax}$  ranges.
- The relationship between simulated SIF and GPP is mainly driven by aPAR. The variance in this relationship is mostly explained by the  $V_{cmax}$  and the chlorophyll content. This highlights the need for better treatment of chlorophyll content in biosphere models.
- The global and regional means as well as the zonal averages of both simulated SIF and GPP are in good agreement with the satellite-based SIF. The seasonality of the satellite-based SIF is quite well reproduced by the simulated SIF and GPP. However, the peaks of the simulated quantities lag by 1 month that of the satellite-based SIF in the Northern and Southern Hemispheres.
- A good agreement is found between the simulated SIF and computed GPP. The relationship is PFT dependent.
- A good agreement is found between the satellite-based SIF and the simulated quantities (SIF and GPP).

The study shows that the models of GPP and SIF in the CCDAS built around SCOPE do not allow us to propagate observations of SIF through constraint of  $V_{cmax}$  to improve estimates of GPP. For this version of CCDAS, this study would rather recommend the use of an empirical relationship between GPP and the satellite-based SIF especially taking account uncertainties in the radiation. Moreover, this empirical approach would be easier to implement and combined with other relevant data for the GPP would help to better estimate this quantity. However, a version of CCDAS which includes the full energy balance (including hydrological scheme) and prognostic photosynthesis (e.g., Knorr et al., 2010; Kaminski et al., 2013) and especially nitrogen scheme may give a slightly different conclusion about the sensitivity of the fluorescence to  $V_{cmax}$ .

**The Supplement related to this article is available online at [doi:10.5194/bg-12-4067-2015-supplement](https://doi.org/10.5194/bg-12-4067-2015-supplement).**

**Acknowledgements.** Rayner is in receipt of an Australian Professorial Fellowship (DP1096309). We are grateful to Christiaan van der Tol for providing the model SCOPE and his initial support. We are also grateful to both Timo Vesala and Dario Papale for providing FLUXNET data at the stations Hyytiala and Roccarespampani 1, respectively.

Edited by: G. Wohlfahrt

## References

- Baldocchi, D. D.: Assessing the eddy covariance technique for evaluating carbon dioxide exchange rates of ecosystems: past, present and future, *Glob. Change Biol.*, 9, 479–492, 2003.
- Beer, C., Reichstein, M., Tomelleri, E., Ciais, P., Jung, M., Carvalhais, N., Rödenbeck, C., Arain, M. A., Baldocchi, D., Bonan, G. B., Bondeau, A., Cescatti, A., Lasslop, G., Lindroth, A., Lomas, M., Luysaert, S., Margolis, H., Oleson, K. W., Rouspard, O., Veenendaal, E., Viovy, N., Williams, C., Woodward, F. I., and Papale, D.: Terrestrial Gross Carbon Dioxide Uptake: Global Distribution and Covariation with Climate, *Science*, 329, 834–838, 2010.
- Berk, A., Anderson, G. P., Acharya, P. K., Chetwynd, J. H., Bernstein, L. S., Shettle, E. P., Matthew, M. W., and Adler-Golden, S. M.: MODTRAN4 USER'S MANUAL, Air Force Research Laboratory, Space Vehicles Directorate, Air Force Materiel Command, Hanscom AFB, MA 01731-3010, 97 pp., 2000.
- Berry, J. A., Frankenberg, C., and Wennberg, P.: New Methods for Measurements of Photosynthesis from Space, KISS report, April, 2013.
- Collatz, G. J., Ball, J. T., Grivet, C., and Berry, J. A.: Physiological and environmental regulation of stomatal conductance, photosynthesis and transpiration: a model that includes a laminar boundary layer, *Agric. For. Meteorol.*, 54, 107–136, 1991.
- Collatz, G., Ribas-Carbo, M., and Berry, J. A.: Coupled photosynthesis-stomatal conductance model for leaves of C4 plants, *Aus. J. Plant Physiol.*, 19, 519–538, 1992.
- Evans, J. R.: Photosynthesis and nitrogen relationships in leaves of C3 plants, *Oecologia*, 78, 9–19, 1989.
- Farquhar, G., Von Caemmerer, S., and Berry, J.: A biochemical model of photosynthetic CO<sub>2</sub> assimilation in leaves of C3 species, *Planta*, 149, 78–90, 1980.
- Flexas, J., Escalona, J. M., Evain, S., Gulías, J., Moya, I., Osmond, C. B., and Medrano, H.: Steady-state chlorophyll fluorescence (Fs) measurements as a tool to follow variations of net CO<sub>2</sub> assimilation and stomatal conductance during water-stress in C3 plants, *Physiol. Plant.*, 114, 231–240, 2002.
- Frankenberg, C., Fisher, J. B., Worden, J., Badgley, G., Saatchi, S. S., Lee, J.-E., Toon, G. C., Butz, A., Jung, M., Kuze, A., and Yokota, T.: New global observations of the terrestrial carbon cycle from GOSAT: Patterns of plant fluorescence with gross primary productivity, *Geophys. Res. Lett.*, 38, L17706, doi:10.1029/2011GL048738, 2011.
- Frankenberg, C., O'Dell, C., Guanter, L., and McDuffie, J.: Remote sensing of near-infrared chlorophyll fluorescence from space in scattering atmospheres: implications for its retrieval and interferences with atmospheric CO<sub>2</sub> retrievals, *Atmos. Meas. Tech.*, 5, 2081–2094, doi:10.5194/amt-5-2081-2012, 2012.
- Jacquemoud, S. and Baret, F.: PROSPECT: A model of leaf optical properties spectra, *Remote Sens. Environ.*, 34, 75–91, 1990.
- Genty, B., Birantais, J., and Baker, N.: The relationship between the quantum efficiencies of photosystems I and II in pea leaves, *Biochem. Biophys. Acta*, 990, 87–92, 1989.
- Ghasemi, K., Ghasemi, Y., Ehteshamnia, A., Nabavi, S. M., Nabavi, S. F., Ebrahimzadeh, M. A., and Pourmorad, F.: Influence of environmental factors on antioxidant activity, phenol and flavonoids contents of walnut (*Juglans regia L.*) green husks, *J. Med. Plants Res.*, 5, 1128–1133, 2011.
- Gilmore, A. M. and Yamamoto, H. Y.: Dark induction of zeaxanthin-dependent non-photochemical fluorescence quenching mediated by ATP, *Proc. Natl. Acad. Sci. USA*, 89, 1899–903, 1992.
- Gilmore, A. M., Mohanty, N., and Yamamoto, H. Y.: Epoxidation of zeaxanthin and antheraxanthin reverses nonphotochemical quenching of photo-system-II chlorophyll-a fluorescence in the presence of trans-thylakoid delta-pH, *FEBS Lett.*, 350, 271–274, 1994.
- Gitelson, A. A., Vinña, A., Verma, S. B., Rundquist, D. C., Arkebauer, T. J., Keydan, G., Leavitt, B., Ciganda, V., Burba, G. G., and Suyker, A. E.: Relationship between gross primary production and chlorophyll content in crops: Implications for the synoptic monitoring of vegetation productivity, *J. Geophys. Res.*, 111, D08S11, doi:10.1029/2005JD006017, 2006.
- Guanter, L., Frankenberg, C., Dudhia, A., Lewis, P. E., Gómez-Dans, J., Kuze, A., Suto, H., and Grainger, R. G.: Retrieval and global assessment of terrestrial chlorophyll fluorescence from GOSAT space measurements, *Remote Sens. Environ.*, 121, 236–251, 2012.
- Houborg R., Cescatti A., Migliavacca, M., and Kustas, W. P.: Satellite retrievals of leaf chlorophyll and photosynthetic capacity for improved modeling of GPP, *Agr. Forest Meteorol.*, 177, 10–23, 2013.
- Joiner, J., Yoshida, Y., Vasilkov, A. P., Yoshida, Y., Corp, L. A., and Middleton, E. M.: First observations of global and seasonal terrestrial chlorophyll fluorescence from space, *Biogeosciences*, 8, 637–651, doi:10.5194/bg-8-637-2011, 2011.
- Joiner, J., Yoshida, Y., Vasilkov, A. P., Middleton, E. M., Campbell, P. K. E., Yoshida, Y., Kuze, A., and Corp, L. A.: Filling-in of near-infrared solar lines by terrestrial fluorescence and other geophysical effects: simulations and space-based observations from SCIAMACHY and GOSAT, *Atmos. Meas. Tech.*, 5, 809–829, doi:10.5194/amt-5-809-2012, 2012.
- Joiner, J., Guanter, L., Lindstrot, R., Voigt, M., Vasilkov, A. P., Middleton, E. M., Huemmrich, K. F., Yoshida, Y., and Frankenberg, C.: Global monitoring of terrestrial chlorophyll fluorescence from moderate-spectral-resolution near-infrared satellite measurements: methodology, simulations, and application to GOME-2, *Atmos. Meas. Tech.*, 6, 2803–2823, doi:10.5194/amt-6-2803-2013, 2013.
- Jung, M., Reichstein, M., Margolis, H.A., Cescatti, A., Richardson, A.D., Arain, M.A., Arneeth, A., Bernhofer, C., Bonal, D., Chen, J., Gianelle, D., Gobron, N., Kiely, G., Kutsch, W., Lasslop, G., Law, B.E., Lindroth, A., Merbold, L., Montagnani, L., Moors, E.J., Papale, D., Sottocornola, M., Vaccari, F., and Williams, C.: Global patterns of land-atmosphere fluxes of carbon dioxide, latent heat, and sensible heat derived from eddy covariance, satellite, and meteorological observations, *J. Geophys.*

- Re.-Biogeosciences, 116, G00J07, doi:10.1029/2010JG001566, 2011.
- Kaminski, T., Knorr, W., Rayner, P., and Heimann, M.: Assimilating atmospheric data into a terrestrial biosphere model: A case study of the seasonal cycle, *Global Biogeochem. Cy.*, 16, 1066, doi:10.1029/2001GB001463, 2002.
- Kaminski, T., Giering, R., Scholze, M., Rayner, P., and Knorr, W.: An example of an automatic differentiation-based modelling system, in: *Computational Science – ICCSA 2003*, edited by: Kumar, V., Gavrilova, L., Tan, C. J. K., and L'Ecuyer, P., International Conference Montreal, Canada, May 2003, Proceedings, Part II, volume 2668 of Lecture Notes in Computer Science, Berlin, Springer, 95–104, 2003.
- Kaminski, T., Rayner, P. J., Voßbeck, M., Scholze, M., and Koffi, E.: Observing the continental-scale carbon balance: assessment of sampling complementarity and redundancy in a terrestrial assimilation system by means of quantitative network design, *Atmos. Chem. Phys.*, 12, 7867–7879, doi:10.5194/acp-12-7867-2012, 2012.
- Kaminski, T., Knorr, W., Schürmann, G., Scholze, M., Rayner, P. J., Zaehle, S., Blessing, S., Dorigo, W., Gayler, V., Giering, R., Gobron, N., Grant, J. P., Heimann, M., Hooker-Strout, A., Houweling, S., Kato, T., Kattge, J., Kelley, D., Kemp, S., Koffi, E. N., Köstler, C., Mathieu, P. P., Pinty, B., Reick, C. H., Rödenbeck, C., Schnur, R., Scipal, K., Sebald, C., Stacke, T., Terwisscha van Scheltinga, A., Vossbeck, Widmann, H., and Ziehn, T.: The BETHY/JSBACH Carbon Cycle Data Assimilation System: experiences and challenges, *J. Geophys. Res.*, 118, 1–13, doi:10.1002/jgrg.20118, 2013.
- Kattge, J., Knorr, W., Raddatz, T. J., and Wirth, C.: Quantifying photosynthetic capacity and its relationship to leaf nitrogen content for global-scale terrestrial biosphere models, *Glob. Change Biol.*, 15, 976–991, 2009.
- Knorr, W.: *Satellite Remote Sensing and Modelling of the Global CO<sub>2</sub> Exchange of Land Vegetation: A synthesis Study*, PhD thesis, Max-Planck-Institute for Meteorology, Hamburg, Germany, Germany, Nr. 49, ISSN 0938-5177, 1997.
- Knorr, W.: Annual and interannual CO<sub>2</sub> exchanges of the terrestrial biosphere: process-based simulations and uncertainties, *Glob. Ecol. Biogeogr.*, 9, 225–252, 2000.
- Knorr, W., Kaminski, T., Scholze, M., Gobron, N., Pinty, B., Giering, R., and Mathieu, P. P.: Carbon cycle data assimilation with a generic phenology model, *J. Geophys. Res.*, 115, G04017, doi:10.1029/2009JG001119, 2010.
- Koffi, E. N., Rayner, P., Scholze, M., and Beer, C.: Atmospheric constraints on gross primary productivity and net ecosystem productivity: Results from a carbon-cycle data assimilation system, *Global Biogeochem. Cy.*, 26, GB1024, doi:10.1029/2010GB003900, 2012.
- Koffi, E. N., Rayner, P. J., Scholze, M., Chevallier, F., and Kaminski, T.: Quantifying the constraint of biospheric process parameters by CO<sub>2</sub> concentration and flux measurement networks through a carbon cycle data assimilation system, *Atmos. Chem. Phys.*, 13, 10555–10572, doi:10.5194/acp-13-10555-2013, 2013.
- Kuze, A., Suto, H., Nakajima, M., and Hamazaki, T.: Thermal and near infrared sensor for carbon observation Fourier-transform spectrometer on the Greenhouse Gases Observing Satellite for greenhouse gases monitoring, *Appl. Opt.*, 48, 6716–6733, 2009.
- Lee, J.-E., Frankenberg, C., van der Tol, C., Berry, J. A., Guanter, L., Boyce, C. K., Fisher, J. B., Morrow, E., Worden, J. R., Asefi, S., Badgley, G., and Saatchi, S.: Forest productivity and water stress in Amazonia: observations from GOSAT chlorophyll fluorescence, *Proc. R. Soc. B*, 280, 20130171, doi:10.1098/rspb.2013.0171, 2013.
- Le Quéré, C., Peters, G. P., Andres, R. J., Andrew, R. M., Boden, T. A., Ciais, P., Friedlingstein, P., Houghton, R. A., Marland, G., Moriarty, R., Sitch, S., Tans, P., Arneeth, A., Arvanitis, A., Bakker, D. C. E., Bopp, L., Canadell, J. G., Chini, L. P., Doney, S. C., Harper, A., Harris, I., House, J. I., Jain, A. K., Jones, S. D., Kato, E., Keeling, R. F., Klein Goldewijk, K., Körtzinger, A., Koven, C., Lefèvre, N., Maignan, F., Omar, A., Ono, T., Park, G.-H., Pfeil, B., Poulter, B., Raupach, M. R., Regnier, P., Rödenbeck, C., Saito, S., Schwinger, J., Segsneider, J., Stocker, B. D., Takahashi, T., Tilbrook, B., van Heuven, S., Viovy, N., Wankinkhof, R., Wiltshire, A., and Zaehle, S.: Global carbon budget 2013, *Earth Syst. Sci. Data*, 6, 235–263, doi:10.5194/essd-6-235-2014, 2014.
- Maxwell, K. and Johnson, G. N.: Chlorophyll fluorescence – a practical guide, *J. Experim. Bot.*, 51, 659–668, 2000.
- Monteith, J. L.: Solar radiation and productivity in tropical ecosystems, *J. Appl. Ecol.*, 9, 747–766, 1972.
- Parazoo, N. C., Bowman, K., Fisher, J. B., Frankenberg, C., Jones, D. B., Cescatti, A., Pérez-Priego, O., Wohlfahrt, G., and Montagnani, L.: Terrestrial gross primary production inferred from satellite fluorescence and vegetation models, *Glob. Change Biol.*, 20, 3103–3121, doi:10.1111/gcb.12652, 2014.
- Papale, D., Reichstein, M., Aubinet, M., Canfora, E., Bernhofer, C., Kutsch, W., Longdoz, B., Rambal, S., Valentini, R., Vesala, T., and Yakir, D.: Towards a standardized processing of Net Ecosystem Exchange measured with eddy covariance technique: algorithms and uncertainty estimation, *Biogeosciences*, 3, 571–583, doi:10.5194/bg-3-571-2006, 2006.
- Rayner, P., Scholze, M., Knorr, W., Kaminski, T., Giering, R., and Widmann, H.: Two decades of terrestrial Carbon fluxes from a Carbon Cycle Data Assimilation System (CCDAS), *Global Biogeochem. Cy.*, 19, GB2026, doi:10.1029/2004GB002254, 2005.
- Rosema, A., Snel, J. F. H., Zahn, H., Buurmeijer, W. F., and van Hove, L. W. A.: The relation between laser-induced chlorophyll fluorescence and photosynthesis, *Rem. Sens. Environ.*, 65, 143–154, 1998.
- Scholze, M., Kaminski, T., Rayner, P., Knorr, W., and Giering, R.: Propagating uncertainty through prognostic carbon cycle data assimilation system simulations, *J. Geophys. Res.*, 112, D17305, doi:10.1029/2007JD008642, 2007.
- Seaton, G. G. and Walker, D. D.: Chlorophyll fluorescence as a measure of carbon metabolism, *Proc. Roy Soc. (London)*, 242, 29–35, 1990.
- Shaahan, M. M., El-Sayed, A. A., and Abou El-Nour, E. A. A.: Predicting nitrogen, magnesium and iron nutritional status in some perennial crops using a portable chlorophyll meter, *Sci. Hortic.*, 82, 339–348, 1999.
- van den Berg, A. K. and Perkins, T. D.: Evaluation of portable chlorophyll meter to estimate chlorophyll and nitrogen contents in sugar maple (*Acer saccharum* Marsh.) leaves, *Forest Ecol. Manage.*, 200, 113–117, 2004.

- van der Tol, C., Verhoef, W., and Rosema, A.: A model for chlorophyll fluorescence and photosynthesis at leaf scale, in: *Agricultural and forest meteorology*, 149, 96–105, 2009a.
- van der Tol, C., Verhoef, W., Timmermans, J., Verhoef, A., and Su, Z.: An integrated model of soil-canopy spectral radiances, photosynthesis, fluorescence, temperature and energy balance, *Biogeosciences*, 6, 3109–3129, doi:10.5194/bg-6-3109-2009, 2009b.
- van der Tol, C., Berry, J. A., Campbell, P. K. E., and Rascher, U.: Models of fluorescence and photosynthesis for interpreting measurements of solar induced chlorophyll fluorescence, *J. Geophys. Res.-Biogeosciences*, 119, 2312–2327, 2014, <http://www.biogeosciences.net/119/2312/2014/>.
- Verhoef, W. and Bach, H.: Coupled soil-leaf-canopy and atmosphere radiative transfer modeling to simulate hyperspectral multi-angular surface reflectance and TOA radiance data, *Remote Sens. Environ.*, 109, 166–182, 2007
- Verhoef, W., Jia, L., Xiao, Q., and Su, Z.: Unified optical-thermal four-stream radiative transfer theory for homogeneous vegetation canopies, *IEEE T. Geosci. Remote*, 45, 1808–1822, 2007.
- Verhoef, W., van der Tol, C., and Middleton, E. M.: Vegetation Canopy Fluorescence and Reflectance Retrieval by Model Inversion Using Optimization, 5th International Workshop on remote sensing of vegetation fluorescence, 22–24 April 2014, Paris, France, <http://www.congrexprojects.com/2014-events/14c04/proceedings>, 2014.
- Weedon, G. P., Gomes, S., Viterbo, P., Shuttleworth, W. J., Blyth, E., Österle, H., Adam, J. C., Bellouin, N., Boucher, O., and Best, M.: Creation of the WATCH Forcing Data and Its Use to Assess Global and Regional Reference Crop Evaporation over Land during the Twentieth Century, *J. Hydrometeorol.*, 12, 823–848, 2011.
- Wilson, M. F. and Henderson-Sellers, A.: A global archive of land cover and soil data for use in general circulation climate models, *J. Climatol.*, 5, 119–143, 1985.
- Yang, X., Tang, J. W., Mustard, J. F., Lee, J. E., Rossini, M., Joiner, J., Munger, J. W., Kornfeld, A., and Richardson, A. D.: Solar-induced chlorophyll fluorescence that correlates with canopy photosynthesis on diurnal and seasonal scales in a temperate deciduous forest, *Geophys. Res. Lett.*, 42, 2977–2987, 2015.
- Zhang, Y., Guanter, L., Berry, J. A., Joiner, J., van der Tol, C., Huete, A., Gitelson, A., Voigt, M., and Köhler, P.: Estimation of vegetation photosynthetic capacity from space-based measurements of chlorophyll fluorescence for terrestrial biosphere models, *Glob. Change Biol.*, 20, 3727–3742, 2014.